Astronomy Reports, Vol. 47, No. 11, 2003, pp. 903–915. Translated from Astronomicheskiĭ Zhurnal, Vol. 80, No. 11, 2003, pp. 978–991.

Spectra, Optical Identifications, and Statistics of a Complete Sample of Radio Sources at Declinations 10°–12°30′

A. G. Gorshkov[1], V. K. Konnikova[1], and M. G. Mingaliev[2]

[1] *Sternberg Astronomical Institute, Universitetskiĭ pr. 13, Moscow, 119992 Russia*

[2] *Special Astrophysical Observatory, Nizhniĭ Arkhyz, Russia*

Received April 7, 2003; in final form, May 8, 2003

Abstract—The results of 0.97, 2.3, 3.9, 7.7, 11.1, and 21.7 GHz observations of a complete sample of radio sources obtained on the RATAN-600 radio telescope are presented. The sample is comprised of sources from the 4.85-GHz MGB survey, and contains all sources at declinations 10°–12°30′ (J2000) with Galactic latitudes $|b| > 15°$ and flux densities $S_{4.85} > 200$ mJy. Optical identifications have been obtained for about 86% of the radio sources with flat spectra and 59% of those with steep spectra. The spectra of the flat-spectrum sources have been decomposed into extended and compact components.

1. ВВЕДЕНИЕ

We are currently studying two complete samples of radio sources. The first sample, which was derived from the Zelenchuk Survey at 3.9 GHz [1], contains all sources in this survey with flux densities $S_{3.9} >$ 200 mJy at declinations 3°30′–6° (B1950); the right ascensions are in the range 0–24^h, and the Galactic latitudes are $|b| > 10°$. This sample contains 160 objects, and we have been studying it since 1984.

The second sample, derived from the GB6 catalog at 4.85 GHz [2], contains all sources from the catalog with flux densities $S_{4.85} > 200$ mJy at declinations 10°–12°30′ (J2000); the right ascensions are in the range 0–24^h, and the Galactic latitudes are $|b| > 15°$. In this sample of 153 objects, 83 have flat spectra with $\alpha_{(3.9-7.7)} > 0.5$ ($S \propto \nu^\alpha$) and 70 have steep spectra with $\alpha_{(3.9-7.7)} < -0.5$.

The main goals of our investigations of these samples are the following:

(1) studying the variability of the sample sources on time scales from several days to several years (observations over the wide frequency range 0.97–21.7 GHz can be used to derive the main characteristics of the variability—its time scale and amplitude, as well as the spectrum of the variable component and the time dependence of its amplitude–frequency characteristics);

(2) deriving the statistical properties of the radio-source spectra;

(3) searching for interesting objects with unusual characteristics in both the radio and optical ranges;

(4) investigating the cosmological evolution of quasars (which requires that redshifts be found for the majority of the optical objects identified with the radio sources).

Daily multi-frequency observations on the RATAN-600 telescope in 1998–1999 confirmed the presence of flux-density variability on time scales of about four days detected earlier [3–5]—so-called intraday variability (IDV). Our studies have shown that such variability is inherent to virtually all flat-spectrum sources, and that IDV is characterized by a flat frequency spectrum with a mean modulation index of about 2% at 2.3–21.7 GHz. Roughly 20% of the objects display significant IDV, as is clearly visible in their structure functions. Several sources show cyclic variability on characteristic time scales of 4–25 days. The statistical properties of the long-term variability of sources in the complete sample and the properties of individual flares for the most active sources have been derived [1, 6].

Various statistical characteristics of the spectra of the sample sources have also been obtained [7, 8]. The unique radio source 0527 + 0331, found to have the most prominent long-term variability, was discovered and studied (all source names are comprised of the first four digits of their right ascension and declination for epoch J2000) [4, 9, 10]. Optical observations aimed at obtaining spectra and redshifts of objects identified with the sample sources to 21^m are ongoing. Studies of the second sample were begun to enable confirmation of the results obtained for the first sample on the basis of a different statistically independent ensemble of radio sources. Up through 2002, three

1063-7729/03/4711-0903$24.00

series of daily multi-frequency observations were carried out for most of the sample sources over 80 days in 2000, 104 days in 2001, and 98 days in 2002.

We present here the first results obtained for the second sample of radio sources.

2. OBSERVATIONS

Meridian observations were carried out on the Northern sector of the RATAN-600 radio telescope at 0.97, 2.3, 3.9, 7.7, 11.1, and 21.7 GHz in June–November 2001. The parameters of the receivers used are presented in [11]. The observations were carried out in a fixed-focus regime, as described in [12]. Readjustment of the main mirror was possible within $\pm 1.25^\circ$ of the center of the declination zone. An equal number of panels of the main mirror were mounted at all altitudes, in order to reduce the influence of variations in the radiation of the outer panels as the curvature of the circular reflector changed. The effective area remained constant over the entire frequency range.

The calibrator for the observations was 1347 + 1217, whose angular size is much smaller than the horizontal cross section of the antenna beam right up to 21.7 GHz. We took the flux density of 1347 + 1217 to be 6.15, 4.12, 3.23, 2.36, 1.99, and 1.46 Jy at 0.97, 2.3, 3.9, 7.7, 11.1, and 21.7 GHz, respectively.

The observations were reduced using a program package that yielded both the flux densities for individual observations and the mean flux density over an entire observing series. The reduction was based on optimal filtration of the input data using the method described in detail in [13]. Before this optimal filtration, non-linear filters were used to clean the input data of impulsive noise, jumps, and trends with time scales longer than the scale of the antenna beam in right ascension. When deriving the mean flux density over an entire observing interval, we used only those recordings for which the noise dispersion at the location of the source belonged to a single general population; the method used to reduce such recordings is described in [14].

The mean flux densities were determined via optimal filtration of the mean recording, whose ith point was the median value of all the ith points of the cleaned input recordings. As a check, we also derived the mean flux density from the relation

$$\bar{S} = \left(\sum_i^n S_i\right)/n, \qquad (1)$$

where S_i is the flux density of the ith observation and n is the number of observations. Introducing a weighting function is superfluous in this case, since only recordings belonging to a single general population were summed.

It is clear that the flux densities obtained in these two ways should be similar, and appreciable differences between them suggest the presence of bad recordings that were not removed during the initial filtration. Our experience demonstrated that such differences arose fairly rarely, testifying to the correctness of the filtration algorithm applied. Bad recordings that were not excluded were primarily those corresponding to observations made with an incorrect antenna setup. If a significant difference was observed, all the recordings were inspected visually and any considered suspicious were excluded, after which the entire reduction procedure was repeated.

The errors in the measurements were determined in two ways:

$$\sigma_\Sigma = \left(\sigma^2 / \sum_i A_i^2\right)^{\frac{1}{2}},$$

where σ^2 is the dispersion of the residual noise in a mean recording after excluding the detected source and A_i is the tabulated antenna beam, and

$$\sigma_s = \left(\left(\sum_i^n (S_i - \bar{S})^2\right)/n(n-1)\right)^{\frac{1}{2}},$$

where $\bar{S}$ is the mean flux density given by (1).

These two estimates should be similar. If they belonged to different general populations (according to the Fisher criterion), we likewise searched for bad recordings. In any case, the larger of the two estimates was adopted as the error in the measured flux density. In this approach to estimating the errors, the errors also include the rms variation of the flux density associated with intrinsic variability of the source during the series of observations.

For several steep-spectrum sources for which significant linear polarization was found in [15], we constructed the flux density using the formula [16]

$$S = 0.5 S_0 [1 + p \cos 2(q - \chi - \psi)],$$

where S_0 is the total flux density of the source, p and q are the degree of linear polarization and the parallactic angle, respectively, χ is the angle between the plane of linear polarization of the receiver and the vertical, and ψ is the position angle of polarization.

3. OPTICAL IDENTIFICATIONS

We used accurate radio coordinates taken primarily from the JVAS (Jodrell Bank–VLA Astrometric Survey) catalog at 8.4 GHz [17] (an rms coordinate error of $0.014''$) and the NVSS (NRAO VLA

Sky Survey) catalog at 1.4 GHz [18] (mean rms coordinate errors of about 0.11″ and 0.56″ for right ascension and declination, respectively). The optical coordinates and B magnitudes were taken from the USNO astrometric survey [19] or APM [20]. A radio source was considered to be identified with an optical object if the difference between the radio and optical coordinates was less than 3σ of the error in the radio range coordinates.

A significant number of objects identified with sources in the sample had been classified earlier. All redshifts and object classifications presented here were obtained from the catalog of quasars and active galactic nuclei [21] published in 2001, the NED extragalactic database [22], and our earlier work [23–25]. Thirteen objects identified with sources in the sample have not yet been classified.

4. RESULTS

4.1. Radio Sources with Steep Spectra and the Flux-density Scale

The sample includes 70 sources with steep spectra. We did not include double-lobed sources whose total flux density at 4.85 GHz was less than 400 mJy in the sample. We did not observe ten sources because either they were larger than the size of the antenna beam at most of the frequencies observed or they were double sources that were unresolved in our observations. Table 1 presents for these sources (1)–(2) their coordinates, (3) classification (as quasars, Q, or galaxies, G), (4) redshifts, (5) references for the redshifts, and (6) B magnitudes.

The spectrum of the calibrator $1347+1217$ at 0.97–21.7 GHz was approximated by a power law, $\log S = A + B\log\nu$. The spectra of 68% of the sources could be approximated well with such linear relations (S spectra), while the spectra of the remaining sources were approximated using parabolas of the form $\log S = A + B\log\nu + C\log^2\nu$.

The spectra of three sources flatten at high frequencies (type C_+), probably due to the presence of a compact component, and the spectra of 15 sources flatten at low frequencies due to synchrotron self-absorption (type C_-); this flattening is most evident at frequencies below 2.3 GHz, while the spectra remain close to linear power laws at higher frequencies.

The flux densities for 36 of the steep-spectrum sources were below our detection limit at 21.7 GHz. The measured flux densities for some of the sources are underestimated, mainly at frequencies higher than 7.7 GHz, because the size of the source was comparable to the size of the antenna beam in right ascension. This underestimation is consistent with the angular sizes given in the Texas 0.365 GHz survey [26].

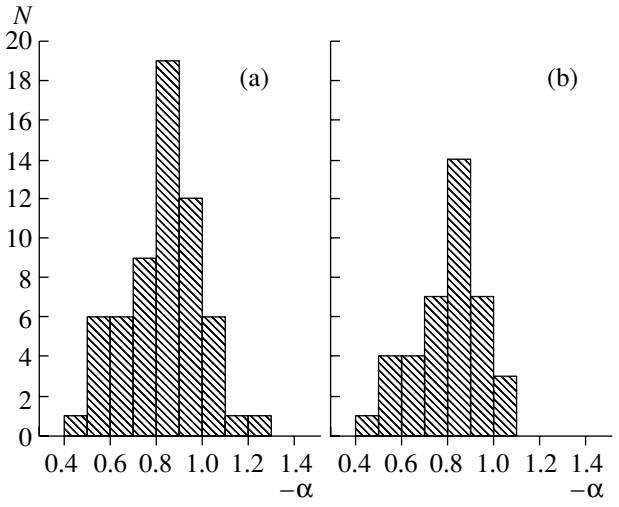

Fig. 1. Distribution of spectral indices for (a) all sources with steep spectra at 3.9 GHz and (b) sources with S spectra.

For these sources, the spectra were approximated using only the data at frequencies where the source angular size was smaller than the antenna beam.

Table 2 presents information about the 60 sources with steep spectra. The columns give the (1)–(2) J2000 coordinates of the objects, (3) optical identifications (quasar, Q, or galaxy, G; a "+" indicates that the source has been identified but a spectrum is not yet available), (4) redshifts, (5) references for the redshifts, (6) B magnitudes, and (7)–(9) coefficients A, B, and C for the approximations to the measured spectra. A star in the last column indicates sources whose angular sizes are comparable to the size of

Table 1. Coordinates and optical identifications of extended radio sources in the sample

Radio coordinates (J2000.0)		Id	z	Ref.	V
R.A.	DEC.				
$02^h17^m07.62^s$	11°04′10.59″	Q	0.408	[21]	15.9
03 58 57.71	10 27 17.76	G	0.031	[21]	15.4
04 13 42.14	11 11 44.82	G	0.306	[21]	19.5
09 14 19.36	10 06 38.28	G	0.311	[25]	19.9
12 29 51.84	11 40 24.09	G	0.083	[22]	16.0
12 30 48.27	12 23 33.07	G	0.004	[21]	12.9
14 16 53.51	10 48 40.06	G	0.024	[22]	13.0
15 14 49.50	10 17 00.74	EF			
22 49 54.59	11 36 30.84	G	0.026	[22]	9.4
23 15 34.40	10 27 18.40	G	0.255	[25]	17.6

Table 2. Optical identifications and approximations of the sample constants

Radio coordinates (J2000.0)		Id	z	Ref.	B	Parameters Approximation			Comments (see text)
R.A.	DEC.					A	B	C	
$00^h29^m08.953^s$	+11°36′28.20″	EF				2.984	−0.792	−0.086	
00 34 56.157	+10 27 52.03	G	0.057	[22]	15.0	3.021	−0.636		*
00 40 50.354	+10 03 23.14	G	0.188	[21]	18.7	3.872	−0.984		
00 44 34.653	+12 11 19.32	G	0.228	[21]	18.9	2.934	−0.832		*
02 20 47.458	+11 21 42.40	EF				3.278	−0.846	−0.108	*
02 38 30.865	+10 10 07.66	G			19.6	3.171	−0.938		
02 45 14.608	+10 47 01.57	EF				2.740	−0.796		
03 15 21.039	+10 12 43.12	G	0.222	[25]	19.6	3.331	−0.925	0.240	
03 27 23.109	+12 08 35.71	EF				3.191	−0.815	0.081	
04 40 12.413	+11 34 03.83	EF				2.998	−0.861	−0.087	
07 28 32.882	+12 10 10.39	EF				3.152	−0.891		
07 45 28.211	+12 09 28.85	EF				3.007	−1.067		
08 04 47.974	+10 15 22.73	Q	1.956	[21]	17.6	3.415	−1.030		
09 06 04.192	+11 03 27.61	G		[25]	19.2	3.011	−0.874		*
10 14 16.028	+10 51 06.16	+			18.7	3.048	−0.673	−0.224	
10 34 05.090	+11 12 31.95	EF				3.175	−0.908		
11 00 47.733	+10 46 12.98	Q	0.420	[21]	17.9	2.954	−0.936		*
11 04 34.802	+11 03 23.90	EF				3.006	−0.792	−0.138	
11 09 46.038	+10 43 43.21	EF				3.244	−0.562	−0.377	
11 26 27.190	+12 20 33.10	G			19.2	3.123	−0.910		
11 30 19.246	+10 15 26.30	EF				2.694	−0.505		
11 40 27.693	+12 03 07.44	G			15.0	3.301	−0.913		
11 53 03.107	+11 07 20.29	EF				3.079	−1.043	−0.116	
11 59 29.114	+10 46 01.00	EF				2.953	−0.920		
12 04 26.711	+11 29 09.68	EF				2.893	−0.766		
12 23 08.875	+10 29 01.05	EF				2.843	−0.643	−0.132	
12 28 36.804	+10 18 41.69	Q	2.305	[21]	19.0	2.941	−0.885		
12 31 19.866	+11 22 45.03	EF				2.979	−0.709	−0.104	
13 06 19.248	+11 13 39.79	G	0.084	[24]	15.4	2.684	−0.605		
13 09 05.161	+10 29 39.91	EF				2.826	−0.786		
13 21 18.844	+11 06 49.25	Q	2.175	[21]	18.4	3.475	−0.778	−0.052	
13 41 04.302	+10 32 05.96	EF				2.902	−0.988		
13 47 33.425	+12 17 23.94	G	0.121	[21]	14.9	3.783	−0.463		
13 52 56.363	+11 07 07.57	EF				3.295	−0.739	−0.353	
14 23 30.103	+11 59 51.24	Q	1.611	[21]	17.5	3.077	−0.635		
15 11 29.436	+10 01 43.73	EF				2.935	−0.874		
15 22 12.151	+10 41 30.35	G	0.204	[25]	21.0	2.783	−0.823		*
15 23 27.563	+11 30 23.76	+			19.1	2.697	−0.555		
15 23 56.936	+10 55 44.02	+			21.1	3.137	−0.786	−0.115	
15 59 06.913	+12 10 26.95	EF				2.839	−0.814		
15 59 16.840	+11 15 46.11	EF				2.926	−0.746		
16 04 05.732	+11 27 59.88	EF				2.871	−0.892		
16 21 10.388	+10 46 13.88	Q	1.305	[25]	21.8	3.107	−0.743	+0.118	

Table 2. (Contd.)

Radio coordinates (J2000.0)		Id	z	Ref.	B	Parameters Approximation			Comments (see text)
R.A.	DEC.					A	B	C	
$16^h31^m45.247^s$	+11°56′02.99″	Q	1.792	[21]	18.2	3.306	−0.582		
16 38 22.118	+10 35 07.74	EF				3.144	−0.614		
16 40 47.989	+12 20 02.08	EF				3.382	−0.414	−0.064	
17 09 35.035	+11 40 27.72	+			18.8	2.865	−0.780		*
17 13 43.382	+10 37 24.86	+			19.3	2.869	−0.749	−0.084	
17 27 53.762	+10 42 56.50	Q	0.833	[21]	20.2	2.784	−0.891		
20 22 08.547	+10 01 10.81	Q	0.469	[21]	19.4	3.651	−0.941		*
21 38 26.222	+11 58 04.15	EF				2.979	−0.940		*
21 51 04.053	+12 19 50.45	EF				3.114	−0.958	−0.070	*
22 01 16.687	+10 23 47.59	Q	1.729	[21]	18.1	2.832	−0.848		
22 03 45.543	+12 17 15.63	+			18.9	2.895	−0.844		
22 29 57.456	+11 27 37.73	G	0.239	[23]	21.2	2.794	−0.783		
22 41 34.421	+11 45 44.84	EF				3.062	−0.841		*
22 54 10.450	+11 36 37.90	Q	0.325	[21]	15.6	3.283	−0.739		
23 11 17.868	+10 08 15.35	Q	0.432	[21]	16.2	2.950	−0.897		*
23 12 10.467	+12 24 03.46	Q	1.285	[25]	19.1	2.842	−0.745		
23 29 41.090	+11 17 28.60	G	0.119	[22]	18.4	2.758	−0.507		

the antenna beam in right ascension at frequencies higher than 7.7 GHz. The flux density of 1140 + 1203 at 3.9 GHz is appreciably lower than the values approximated using the remaining data.

Figure 1 shows the distribution of spectral indices for (a) all the sources and (b) the sources with type S spectra. The mean spectral index for the sources with S spectra is $\bar{\alpha} = -0.808$ with an rms deviation of $\sigma = 0.15$, while the mean spectral index at 3.9 GHz for all the sources is $\bar{\alpha} = -0.815$ with an rms deviation of $\sigma = 0.17$. In [7], we obtained for the steep-spectrum sources in a sample at declinations $3°30' - 6°$ (B1950) the mean spectral index $\bar{\alpha} = -0.857$ with an rms deviation of $\sigma = 0.14$. After taking into account sources that were obviously resolved by the antenna beam, this value decreased to $\bar{\alpha} = -0.81$, which is virtually identical to the mean spectral index obtained for our second sample in a different range of declinations.

The mean ratio of our 1.4-GHz flux densities and the flux densities from the NVSS survey [18] for all the steep-spectrum sources with sizes much less than the size of the antenna beam below 11.1 GHz is $S_{app1.4}/S_{\rm NVSS} = 1.019 \pm 0.004$. The mean ratio of our 4.85-GHz flux densities and the flux densities of the GB6 survey is $S_{app4.85}/S_{\rm GB6} = 1.09 \pm 0.01$. On average, our flux-density estimates for 0.365 GHz are in agreement with those in the Texas survey, although the accuracy of our approximations outside the range of our observed frequencies is lower than the accuracy within this range.

Of the 70 steep-spectrum radio sources, 21 are identified with galaxies (17 of which have measured redshifts), 14 are identified with quasars, and 29 are in empty fields to 21^m. The spectra of six objects have not yet been obtained. Figure 2 shows the redshift distributions of the galaxies and quasars. The mean redshift of the galaxies is $\bar{z}(\mathrm{G}) = 0.15$ ($\sigma = 0.1$), while that of the quasars is $\bar{z}(Q) = 1.22$ ($\sigma = 0.7$).

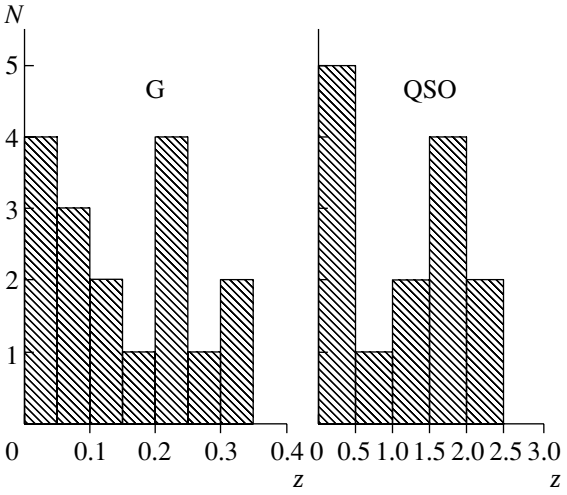

Fig. 2. Redshift distribution of galaxies and quasars identified with steep-spectrum sources.

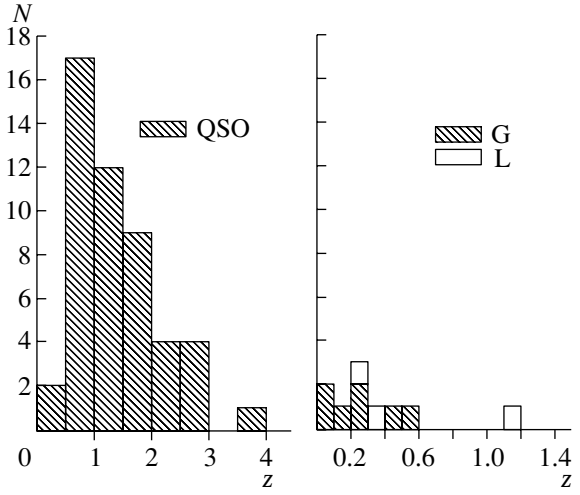

Fig. 3. Redshift distribution for the quasars, galaxies, and BL Lac objects identified with flat-spectrum sources in the sample.

4.2. Flat-spectrum Radio Sources ($\alpha > -0.5$)

Table 3 presents for the flat-spectrum sources their (1)–(2) J2000 radio coordinates, (3) optical identifications, (4) redshifts, (5) references for the redshifts, (6) B magnitudes, and (7)–(18) flux densities and rms measurement errors. Flux densities were obtained at six frequencies for all these sources except $2203+1007$, whose flux density at 0.97 GHz does not exceed 70 mJy, and $0448+1127$, whose 7.7 GHz flux density we were not able to estimate because the neighboring strong source $0449+1121$ fell in the second feed horn. The flux densities of $0449+1121$ and $1728+1215$ are significantly and rapidly variable, and the table presents the spectra obtained on June 5, 2001 and August 30, 2001, respectively.

Of the 83 flat-spectrum objects in the complete sample, 72 (86%) have optical identifications, and 11 are in empty fields to 21^m. The spectrum of the optical object identified with $1603+1105$ is stellar, probably because the real optical object is blended with a star. Forty-nine of the sources are classified as quasars and eight as galaxies (seven of which have measured redshifts). Seven sources are BL Lac objects (three of which have measured redshifts), among them $0409+1217$, $0757+0956$, and $1309+1154$, which have high degrees of polarization in the radio. Six objects have not yet been classified.

Figure 3 presents the redshift distribution of the quasars, galaxies, and BL Lac objects. The mean redshift of the quasars is $\bar{z}(\mathrm{Q}) = 1.40$ (rms deviation $\sigma(\mathrm{Q}) = 0.74$), of the BL Lac objects is $\bar{z}(\mathrm{L}) = 0.55$ ($\sigma(\mathrm{L}) = 0.40$), and of the galaxies is $\bar{z}(\mathrm{G}) = 0.26$ ($\sigma(\mathrm{G}) = 0.19$).

Figure 4 shows the redshift dependence of the absolute spectral luminosity at 11.1 GHz for the flat-spectrum sources in the sample calculated for a uniform, isotropic cosmological model with a zero cosmological constant, deceleration parameter $q = 0.5$, and $H = 50$ km s^{-1}Mpc^{-1}. The solid line represents the minimum luminosity that can be detected for the given flux-limited sample.

Most of the flat-spectrum sources are composed of at least two components—an extended one and a compact one.

To study the characteristics of the spectra of compact components, we must isolate these spectra by excluding the contribution of any extended components. Here, when we refer to the "compact component," we mean the total radiation of the jet, which is made up of clouds of relativistic electrons that have formed as a result of propagating shock waves and are located in various stages of their evolution. The formation and evolution of these clouds under the action of shocks in the relativistic jet plasma is thought to give rise to the observed variability of extragalactic radio sources [27–29]. Valtaoya *et al.* [30] present a semi-quantitative analysis of a "generalized model" that can be applied to trace the evolution of the spectral and temporal characteristics of flares occurring at various stages of the interaction of a shock front and cloud of relativistic electrons.

Spectra covering more than six decades in frequency are constructed in [31] based on nearly coordinated, simultaneous observations carried out from 20 cm to 1400 Å. The spectra of active sources are smooth, and are fit well by a parabolic dependence on a logarithmic scale. At the same time, the spectra of sources with low activity are less smooth and poorly

Table 3. Identifications and flux densities of flat-spectrum sources

Radio coordinates (J2000.0)		Id	z	Ref.	B	Flux density and its error, mJy											
R.A.	DEC.					0.97 GHz		2.3 GHz		3.9 GHz		7.7 GHz		11.1 GHz		21.7 GHz	
$00^h07^m55.710^s$	$+10°27'43.89''$	EF				310	25	300	11	285	4	262	6	255	8	225	10
00 10 31.007	+10 58 29.51	G	0.089	[21]	14.1	90	15	148	10	182	2	257	3	354	4	650	20
00 36 23.767	+10 07 57.43	Q	1.909	[21]	17.2	822	25	553	10	501	7	483	10	490	10	500	26
00 37 26.042	+11 09 50.91	EF				235	20	235	14	230	9	215	4	223	4	226	10
00 38 18.017	+12 27 31.25	Q	1.395	[21]	16.5	1196	26	781	10	683	6	564	6	539	6	440	22
00 42 44.371	+10 09 49.19	EF				257	20	252	18	243	6	215	6	230	7	210	20
01 21 29.001	+11 27 00.53	Q	2.487	[23]	19.7	88	15	150	15	186	6	210	6	181	11	150	20
01 21 41.595	+11 49 50.42	Q	0.570	[21]	19.2	1532	20	1704	17	1779	18	1948	13	2030	14	1996	45
01 43 31.090	+12 15 42.95	Q	1.178	[25]	19.7	348	15	220	10	173	3	136	4	128	2	110	10
02 03 46.657	+11 34 45.39	Q	3.610	[21]	19.4	682	24	882	11	902	5	984	7	1039	8	1060	32
02 11 13.177	+10 51 34.79	L		[23]	15.1	160	15	297	9	317	5	333	5	364	5	420	20
02 25 41.910	+11 34 25.47	Q	0.924	[21]	17.9	380	22	361	8	333	4	280	5	282	4	303	15
02 42 29.171	+11 01 00.72	Q	2.694	[25]	19.3	1690	25	1341	15	1166	7	1156	9	1266	9	1357	43
03 02 30.548	+12 18 56.77	EF				514	29	536	18	501	5	415	7	361	10	232	20
03 09 03.625	+10 29 16.34	Q	0.863	[21]	18.4	459	24	544	12	651	8	835	9	1018	10	1500	30
03 21 53.104	+12 21 13.95	Q	2.670	[21]	19.4	2000	36	1844	19	1748	4	1442	10	1471	10	1487	40
03 45 01.317	+12 18 48.77	Q	0.901	[23]s	19.5	430	15	296	10	205	3	158	3	149	3	147	14
03 55 45.553	+12 31 46.14	Q	1.616	[21]	18.2	960	21	595	10	527	5	443	5	398	5	333	17
04 09 22.009	+12 17 39.85	L	1.020	[21]	19.2	1003	26	1076	15	938	9	814	7	775	7	723	20
04 44 12.467	+10 42 47.29	Q	2.400	[25]	19.0	820	32	596	18	500	13	377	5	340	8	250	30
04 48 50.413	+11 27 54.39	Q	1.375	[25]	19.4	92	15	178	15	230	11	–	–	280	11	260	20
04 49 07.672	+11 21 28.63	Q	1.207*	[21]	19.9	689	24	1279	15	1732	21	2573	29	3235	30	4377	115
05 09 27.457	+10 11 44.59	L		[25]	19.2	663	20	552	12	464	5	467	10	490	8	589	21
05 16 46.646	+10 57 54.77	Q	1.580	[25]	19.1	1330	20	940	12	818	5	655	6	583	6	470	20
07 45 33.060	+10 11 12.69	EF				2503	35	3930	30	3726	23	2956	22	2502	20	1831	40
07 49 27.385	+10 57 33.12	G	0.214	[25]	19.1	219	43	180	15	182	4	169	9	165	11	126	15
07 50 52.047	+12 31 04.83	Q	0.889	[21]	17.7	1401	34	1385	39	1516	31	1875	32	2370	21	3252	70
07 57 06.640	+09 56 34.80	L	0.280	[21]	14.7	1089	41	1121	12	1130	9	1320	11	1433	17	1536	56
07 58 07.658	+11 36 46.05	G	0.573	[25]	16.0	557	30	393	20	346	5	298	7	294	7	250	20
08 27 06.513	+10 52 24.15	Q	2.295	[21]	17.8	185	20	144	12	141	5	138	5	127	7	150	25

Table 3. (Contd.)

Radio coordinates (J2000.0)		Id	z	Ref.	B	Flux density and its error, mJy											
R.A.	DEC.					0.97 GHz		2.3 GHz		3.9 GHz		7.7 GHz		11.1 GHz		21.7 GHz	
$08^h32^m38.478^s$	$+10°40'19.68''$	EF				193	24	254	15	210	8	191	5	183	10	230	20
08 33 14.368	+11 23 36.25	Q	2.979	[21]	18.3	724	30	351	7	351	3	290	3	274	3	253	10
09 45 49.860	+12 05 31.32	+			19.3	553	28	358	17	308	4	246	6	250	8	262	24
09 46 35.069	+10 17 06.13	Q	1.007	[24]	18.7	358	20	352	10	338	4	280	3	250	3	181	16
09 47 45.857	+11 13 53.99	Q	1.760	[21]	18.1	278	25	230	15	215	5	187	6	168	10	134	15
10 01 57.735	+10 15 49.70	Q	1.530	[21]	17.7	352	20	321	11	299	3	267	3	266	4	226	11
10 02 52.846	+12 16 14.59	+			19.6	207	20	250	11	302	6	360	8	401	13	405	20
10 15 44.024	+12 27 07.07	L		[24]	19.2	185	31	232	11	277	3	367	4	446	5	532	27
10 42 44.530	+12 03 31.73	Q	1.028	[21]	17.5	4191	33	2435	20	1750	12	1230	10	1049	9	766	11
11 03 03.530	+11 58 16.61	Q	0.917	[24]	18.9	305	20	293	7	320	4	345	6	388	5	474	20
11 18 57.302	+12 34 41.72	Q	2.118	[21]	17.9	2410	25	1836	17	1690	15	1534	15	1591	14	1543	38
11 32 59.491	+10 23 42.63	Q	0.540	[21]	16.9	1154	25	617	10	443	4	364	4	375	4	364	19
12 07 12.625	+12 11 45.88	Q	0.896	[24]	19.0	112	20	224	10	260	9	265	9	281	5	318	18
12 18 26.094	+11 05 05.27	Q	1.403	[21]	19.0	247	33	222	8	217	2	283	3	352	3	335	18
12 54 38.256	+11 41 05.89	Q	0.870	[21]	16.1	730	24	706	12	682	10	746	6	888	7	924	30
13 09 33.933	+11 54 24.56	L		[21]	18.5	850	23	990	12	1062	6	1170	8	1238	10	1248	30
13 15 01.853	+12 20 52.63	G	0.261	[24]	18.7	298	20	245	18	219	8	205	10	210	7	215	20
13 27 54.465	+12 23 11.16	Q	0.950	[25]	19.5	560	30	420	15	411	9	405	10	409	8	415	20
14 30 09.739	+10 43 26.86	Q	1.710	[21]	17.8	220	30	624	09	889	5	916	7	911	8	778	29
14 44 50.736	+11 31 56.40	Q	0.851	[21]	17.9	367	20	211	10	160	4	120	7	110	7	98	10
14 53 44.241	+10 25 57.57	Q	1.770	[25]	20.5	383	15	361	10	295	4	195	4	161	2	102	14
14 55 55.418	+11 51 45.86	EF				450	30	327	10	222	6	172	8	146	6	115	18
15 04 24.980	+10 29 39.20	Q	1.833	[21]	18.8	1687	29	1637	14	1745	10	2136	16	2388	18	2540	76
15 07 21.882	+10 18 44.99	G			13.5	340	30	295	15	252	4	176	6	144	7	98	15
15 25 02.936	+11 07 44.09	Q	0.331	[21]	17.4	450	15	361	07	223	2	284	3	283	3	282	18
15 50 43.595	+11 20 47.45	Q	0.436	[21]	16.3	1042	20	544	13	390	4	279	5	252	8	220	20
15 55 43.044	+11 11 24.38	L	0.360	[21]	14.5	314	15	300	08	274	3	328	3	355	4	419	17
16 03 41.930	+11 05 48.68				18.3	185	25	194	12	215	7	237	4	254	6	257	30
16 08 46.203	+10 29 07.78	Q	1.226	[21]	17.8	1671	34	2217	20	2711	17	3286	27	3714	37	4258	133
16 27 37.032	+12 16 07.11	Q	1.216	[25]	18.2	348	30	294	13	275	7	259	11	252	7	220	20
16 40 58.892	+11 44 04.23	G	0.078	[22]	15.6	481	36	315	16	276	9	231	6	219	14	230	36

Table 3. (Contd.)

Radio coordinates (J2000.0)		Id	z	Ref.	B	Flux density and its error, mJy											
R.A.	DEC.					0.97 GHz		2.3 GHz		3.9 GHz		7.7 GHz		11.1 GHz		21.7 GHz	
$16^h45^m54.675^s$	+11°13′52.64″	EF				583	20	365	10	301	4	246	6	239	8	250	30
17 06 20.498	+12 08 59.81	+			19.0	115	17	159	07	187	2	199	3	197	3	173	11
17 22 44.582	+10 13 35.77	Q	0.732	[25]	21.6	380	30	378	18	374	7	370	6	369	12	351	34
17 28 07.051	+12 15 39.48	Q	0.588	[25]	21.7	256	20	405	08	524	6	611	8	635	10	680	29
17 46 56.965	+11 27 17.35	EF				555	20	345	10	290	4	260	3	249	4	195	10
20 31 54.995	+12 19 41.34	Q	1.215	[21]	18.2	875	17	876	13	902	6	850	8	914	8	1034	20
20 35 22.334	+10 56 06.78	Q	0.601	[21]	16.6	1156	25	780	20	785	11	842	10	942	10	1040	47
20 49 45.865	+10 03 14.40	EF				185	20	434	08	500	3	480	4	492	4	511	22
21 23 13.359	+10 07 54.96	Q	0.932	[21]	18.1	930	30	646	10	513	3	403	4	368	3	336	18
21 45 18.776	+11 15 27.30	Q	0.550	[21]	18.0	364	18	368	07	413	4	460	4	499	5	571	16
21 57 12.862	+10 14 24.80	Q	0.761	[21]	18.4	215	20	272	12	267	3	269	4	318	2	428	16
22 00 07.933	+10 30 07.90	+			21.7	300	20	269	12	296	8	319	5	344	10	358	26
22 03 30.953	+10 07 42.58	EF						220	13	325	3	276	3	215	3	102	10
22 22 52.991	+12 13 49.82	+			20.9	290	15	260	15	252	2	230	3	228	3	200	10
22 32 36.409	+11 43 50.89	Q	1.037	[21]	17.1	7822	47	6297	26	5316	28	4266	36	4264	40	4686	70
22 33 58.450	+10 08 52.10	Q	1.854	[23]	17.6	395	25	320	24	360	13	350	10	315	18	275	20
23 00 18.317	+10 37 54.08	Q	2.816	[23]	19.3	79	10	130	10	168	4	159	9	161	7	148	15
23 10 28.517	+10 55 30.68	G	0.494	[25]	18.9	303	18	274	8	447	5	357	4	395	4	427	22
23 30 09.952	+12 28 28.60	G	0.144	[23]	17.5	510	26	343	19	269	6	206	5	190	8	153	20
23 30 40.853	+11 00 18.71	Q	1.489	[21]	17.8	1180	20	1255	20	1183	10	1053	10	1026	10	923	14
23 47 36.406	+11 35 17.89	+			18.3	468	40	267	20	220	5	183	5	186	6	153	20
23 50 02.031	+11 06 36.71	+			19.7	275	15	256	6	257	2	269	3	279	3	280	17

The optical spectrum of the object identified with the source 0449+1121 was obtained on the 6-m telescope of the Special Astrophysical Observatory of the Russian Academy of Sciences. The spectrum shows only a continuum, with no lines, and we have classified the object as a BL Lac object [25]. The references to the redshift presented in the 2001 catalog of quasars and active galaxies ($z = 1.207$) do not include observational data for this object.

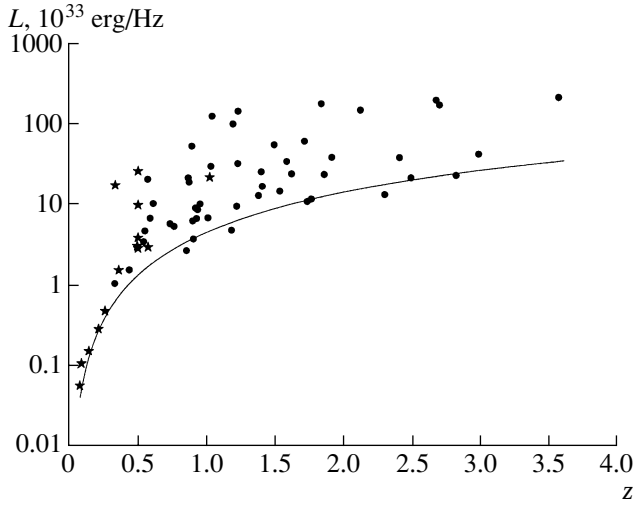

Fig. 4. Redshift dependence of the absolute spectral luminosity at 11.1 GHz for flat-spectrum sources from the sample. The stars denote BL Lac objects and galaxies, while the circles denote quasars. See text for an explanation of the solid curve.

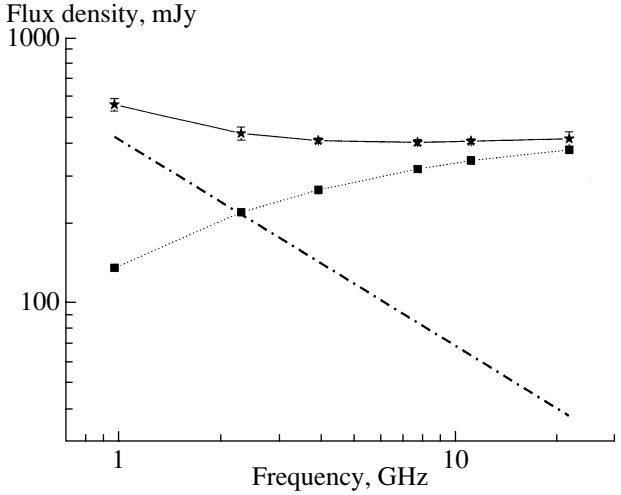

Fig. 5. Decomposition of the spectrum of 1327 + 1223 in June 2001. The solid curve shows the observed spectrum, the dotted curve the spectrum of the compact component, and the dot–dash curve the spectrum of the extended component.

described by parabolic fits. The spectra of variable sources at various stages of development of the variability are studied in [32] based on data obtained in 1965–1973 at 6.6 and 10.7 GHz [33], in 1965–1984 at 4.8, 8.0, and 14.5 GHz [34], and from 1978 to the present at millimeter wavelengths [35]. These spectra are also approximated well by logarithmic parabolas.

In our subsequent analysis, we assume that the spectra of the radio sources are comprised of two components: a power-law component of the form

$$\log S = S_0 + \alpha \log \nu$$

and a compact component that can be represented by a quadratic function of the form

$$\log S = C + 0.5(\log \nu - B)^2/A,$$

where C is the logarithm of the peak flux density, B is the logarithm of the peak frequency, and A is the logarithmic interval from the peak frequency to the frequency at which $d \log S/d \log \nu = 1$ (the curvature parameter of the spectrum) [31].

We decomposed the spectra into components by finding the solution with the minimum residual

$$\sum [S_{\nu i} - (S^s_{\nu i} + S^c_{\nu i})]^2,$$

where $S_{\nu i}$ is the measured flux density at the given frequency, $S^s_{\nu i}$ the flux density of the power-law component, and $S^c_{\nu i}$ the flux density of the compact component. We went through this procedure for nearly all the sources using the data at 0.365 GHz [26].

We believe that the spectral characteristics of the extended components of flat-spectrum and steep-spectrum sources are similar. Accordingly, we considered the decomposition to be successful if the spectral index for the extended component lay in the range $\alpha = -0.5 \ldots -1.1$. The spectra of the extended components were assumed to remain constant over all observing epochs.

We present the characteristics of the spectra at epochs June–November 2001 below. We considered variations of these characteristics within only a narrow time interval from this epoch (one year).

The spectra of the sample sources can be divided into four groups.

(1) The spectra of 28 sources can be described with two components: an extended component with a power-law spectrum and a compact component that is approximated well by a logarithmic parabola with its maximum at a frequency no higher than 25 GHz. The spectrum of the extended component can be determined more accurately. The mean spectral index for the extended components is $\bar{\alpha} = -0.79$, which is close to the mean spectral index obtained for the steep-spectrum sources in the sample, confirming the correctness of the procedure used for the spectral decomposition.

Figure 5 shows the spectral decomposition for 1327 + 1223 as an example, while Fig. 6 show the decompositions for 2035 + 1056 at epochs (a) June 2002 and (b) June 2001.

For 23 objects, the extended component comprises from 18% (1706 + 1208) to 100% (1042 + 1203) of the total flux density at 0.97 GHz. The extended

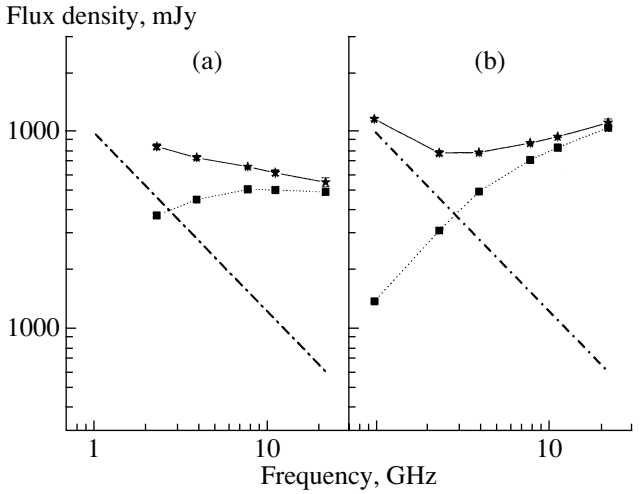

Fig. 6. Same as Fig. 5 for 2035 + 1056 at epochs (a) June 2002 and (b) June 2001.

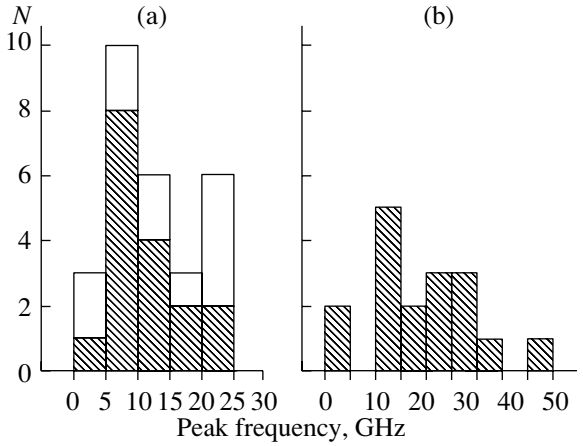

Fig. 7. Distribution of the peak frequencies of the compact components (a) in the rest frame of the observer and (b) in the rest frame of the source. The shaded region in the left diagram corresponds to sources with measured redshifts.

components of five of the objects, such as 0121 + 1127 and 2203 + 1007, are small.

The mean redshift of the quasars of this group is $\bar{z} = 1.58$, with an rms deviation of $\sigma = 0.61$. Figure 7 shows the distribution of the peak frequencies of the compact components in the rest frames of the observer and source. The observed quasar peak frequencies show a dependence on redshift: $\bar{\nu}_{\max} = 8.5$ GHz for quasars with redshifts $z > 1.3$ and $\bar{\nu}_{\max}$=14 GHz for those with $z < 1.3$. In the rest frame of the source, this dependence disappears, and the mean peak frequencies for these redshifts become 25 and 26 GHz, respectively. We did not find any statistically significant correlations between the approximation coefficients for the compact components in the source rest frame and the dependences of these coefficients on the absolute spectral radio luminosity of the source. This same result was obtained for the compact components of sources with declinations 3°30′–6° [8].

The flux densities of most of the sources in this group vary slowly, and their variability indices $V = (S_{\max} - S_{\min})/(S_{\max} + S_{\min})$ do not exceed 0.05. An exception is 1722 + 1013, whose flux density displays appreciable variability, with the variability index at 21.7 GHz being $V = 0.32$ over six months. In November 2001, the observed spectrum of this source rose with frequency, and the spectrum maximum was located beyond our observing interval. The time variations in the spectra of most sources are characterized by a shift of the maximum toward lower frequencies during the evolution of an isolated flare.

(2) The spectra of 22 sources can be decomposed into a power-law component and a parabolic component whose peak frequency is appreciably higher than our highest frequency. The mean spectral index and rms deviation for the extended components of this group do not differ from those for the previous group. The mean redshift for the quasars and BL Lac objects of this group is $\bar{z} = 0.99$, with an rms deviation of $\sigma = 0.57$. The accuracy of the approximation is not sufficiently high to permit quantitative estimates. This group includes more active sources, a large fraction of which have their spectral maxima at frequencies above 30 GHz. The time variations of the spectra of such sources are characterized by variations in the spectral index corresponding to the section of the parabola that grows with frequency. For example, the spectral index of the compact component of 1015 + 1227 between 7.7 and 11.1 GHz varied from +0.38 to +0.55 over three years. The peak frequencies of the compact components of the three sources of this group with the highest redshifts [1118 + 1234 ($z = 2.118$), 1504 + 1029 ($z = 1.883$), and 1608 + 1029 ($z = 1.226$)] are at frequencies lower than 25 GHz at other observing epochs. The spectrum of the compact component of the galaxy 0010 + 1058 in September 2000 can also be approximated by a parabola with its maximum within our frequency range (10 GHz). Seven sources in this group have prominent extended components in our frequency range, and we can detect the compact component only at our highest frequencies.

There is no fundamental difference between the first and second group of sources, and the peak frequencies are distributed fairly uniformly when observations over a broader range of frequencies are considered. The higher activity of sources in the second group is associated with their higher peak frequencies [30].

(3) The spectra of 17 sources cannot be decomposed using two-component models. We believe that their spectra include contributions from several compact components. The measured points in the spectra are insufficient to enable an unambiguous decomposition into components. Only for two sources whose extended components were weak and for which there were observations at 0.365 GHz were we able to separate their spectra into two components, each of which has a parabolic spectrum. For example, the spectrum of $1453+1025$ is the superposition of two parabolas with their maxima at 1.3 and 20 GHz. Most sources in this group remained complex at all observing epochs. The mean redshift of the quasars is $\bar{z}=1.76$, with rms deviation $\sigma=0.87$. Many sources display appreciable flux-density variability at high frequencies, $V_{21.7}>0.13$ over a year. Several sources also display appreciable variability at low frequencies, comparable in amplitude to the variability at high frequencies. For example, the variability index of $0409+1217$ at 2.3 GHz is $V=0.33$, while the variability index at 21.7 GHz is $V=0.29$. More than half of the BL Lac objects belong to this group.

(4) The 0.365–21.7 GHz spectra of 11 sources either can be approximated by a power law with an index from $\alpha=-0.04$ $(0037+1109)$ to $\alpha=-0.5$ $(1455+1151,\ 1507+1018)$ or flatten at frequencies above 3.9 GHz. This flattening is probably due to a compact component that is present at higher frequencies, although it is not possible to separate out the spectral components of these sources using the model considered. Sixty per cent of the identified sources in this group are galaxies, and sources that were observed more than once do not display significant variability.

We were not able to interpret the spectra of $0833+1123$ and $2310+1055$. There are no flux-density measurements for the former source at frequencies below 0.97 GHz, while our observations show a flux density at 0.97 GHz of 724 mJy. In the case of the latter source, a nearby source falls into the antenna beam at several frequencies.

5. CONCLUSION

We have derived flux densities in the range 0.97–11.1 GHz for all the sample sources with steep spectra and up to 21.7 GHz for one third of the spectra. The spectra of 68% of the sources can be approximated with power laws over this entire frequency range, and the spectra of 28% of the sources display self-absorption at low frequencies. The spectra of three sources flatten toward high frequencies, probably due to the presence of compact components whose peak frequencies are above our studied frequency range.

We have also derived 0.97–21.7 GHz flux densities for all the sample sources with flat spectra, and divided their spectra into extended and compact components. The extended components can be approximated by logarithmic power laws with spectral indices $\alpha=-0.5\ldots-1.1$, while the compact components were described using logarithmic parabolas. We were able to obtain a satisfactory spectral decomposition for 50 sources, consistent with available flux-density measurements at low frequencies. The contribution of the extended component at 0.97 GHz can range from 0 to 100% for various sources. The spectra of 17 sources could not be decomposed using such two-component models, probably because they include the contributions of several compact components.

We found no statistically significant correlations between the spectral parameters and the absolute spectral radio luminosities of compact components whose peaks are below 25 GHz in the source rest frame.

All the sources have been optically identified. A significant number of the optical objects associated with the sample sources were classified earlier; work on obtaining optical spectra of the remaining optical objects is ongoing.

Fifty-nine per cent of the steep-spectrum sources are identified to 21^m; among these, 52% are galaxies with a mean redshift of $\bar{z}=0.15$, 34% are quasars with $\bar{z}=1.22$, and the spectra of six objects have not yet been obtained.

Eighty-six per cent of the flat-spectrum sources have optical identifications; among these, 68% are quasars with a mean redshift of $\bar{z}=1.40$, 10% are BL Lac objects with $\bar{z}=0.55$, 11% are galaxies with $\bar{z}=0.26$, and the remaining objects have not yet been classified.

6. ACKNOWLEDGMENTS

This work was supported by the Russian Foundation for Basic Research (project no. 01-02-16331), a grant of the "Universities of Russia" program (project no. УР.02.03.005), and a grant from the State Science and Technology Program "Astronomy."

REFERENCES

1. A. G. Gorshkov and V. K. Konnikova, Astron. Zh. **72**, 291 (1995) [Astron. Rep. **39**, 257 (1995)].
2. P. C. Gregory, W. K. Scott, K. Douglas, and J. J. Condon, Astrophys. J., Suppl. Ser. **103**, 427 (1996).
3. D. S. Heeschen, Astron. J. **89**, 1111 (1984).
4. A. G. Gorshkov, V. K. Konnikova, and M. G. Mingaliev, Astrophys. Space Sci. **278**, 93 (2001).
5. A. G. Gorshkov, V. K. Konnikova, M. G. Mingaliev, *et al.*, Astron. Zh. (in preparation).

6. A. G. Gorshkov, V. K. Konnikova, and M. G. Mingaliev, Astron. Zh. (in preparation).
7. A. M. Botashev, A. G. Gorshkov, V. K. Konnikova, and M. G. Mingaliev, Astron. Zh. **76**, 723 (1999) [Astron. Rep. **43**, 631 (1999)].
8. A. G. Gorshkov, V. K. Konnikova, and M. G. Mingaliev, Astron. Zh. **77**, 407 (2000) [Astron. Rep. **44**, 353 (2000)].
9. A. G. Gorshkov and V. K. Konnikova, Astron. Zh. **74**, 374 (1997) [Astron. Rep. **41**, 325 (1997)].
10. A. G. Gorshkov, V. K. Konnikova, and M. G. Mingaliev, Astron. Zh. **77**, 188 (2000) [Astron. Rep. **44**, 161 (2000)].
11. A. B. Berlin, A. A. Maksyasheva, N. A. Nizhel'skiĭi, *et al.*, in *Abstracts of the XXVII Radio Astronomy Conference, St. Petersburg* (1997), Vol. 3, p. 115.
12. N. S. Soboleva, A. V. Temirova, and T. V. Pyatununa, Preprint Spets. Astrofiz. Obs. (1986).
13. A. G. Gorshkov and O. I. Khromov, Astrofiz. Issled. (Izv. SAO) **14**, 15 (1981).
14. A. G. Gorshkov and V. K. Konnikova, Astron. Zh. **73**, 351 (1996) [Astron. Rep. **40**, 314 (1996)].
15. H. Tabara and M. Inoue, Astron. Astrophys., Suppl. Ser. **39**, 379 (1980).
16. A. D. Kuz'min and A. E. Solomonovich, *Radio Astronomical Methods for the Measurement of Antenna Parameters* [in Russian] (Sov. Radio, Moscow, 1964).
17. I. W. A. Browne, Mon. Not. R. Astron. Soc. **293**, 257 (1998).
18. J. J. Condon, W. D. Cotton, E. W. Greisen, *et al.*, Astron. J. **115**, 1693 (1998).
19. D. Monet, A. Bird, B. Canzian, *et al.*, *USNO-SA1.0* (U.S. Naval Obs., Washington, 1996).
20. R. L. Pennington, R. M. Humphreys, S. C. Odewahn, *et al.*, Publ. Astron. Soc. Pac. **105**, 103 (1993).
21. M. P. Veron-Cetty and P. Veron, Astron. Astrophys. **374**, 92 (2001).
22. NASA/IPAC Extragalactic Database. http://nedwww.ipac.caltech.edu.
23. V. Chavushyan, R. Mujica, J. R. Valdes, *et al.*, Astron. Zh. **79**, 771 (2002) [Astron. Rep. **46**, 697 (2002)].
24. V. L. Afanas'ev, S. N. Dodonov, A. V. Moiseev, *et al.*, Astron. Zh. **47**, 6 (2003) [Astron. Rep. **47**, 458 (2003)].
25. V. L. Afanas'ev, S. N. Dodonov, A. V. Moiseev, *et al.*, Astron. Zh. (in preparation).
26. J. N. Douglas, Bull. Am. Astron. Soc. **19**, 1048 (1987).
27. R. D. Blandford and A. Königl, Astrophys. J. **232**, 34 (1979).
28. A. H. Marscher and W. K. Gear, Astrophys. J. **298**, 114 (1985).
29. P. A. Hughes, H. D. Aller, and M. F. Aller, Astrophys. J. **374**, 57 (1991).
30. E. Valtaoya, H. Terasranta, S. Urpo, *et al.*, Astron. Astrophys. **254**, 71 (1992).
31. R. Landau, B. Golisch, T. J. Jones, *et al.*, Astrophys. J. **308**, 78 (1986).
32. A. G. Gorshkov, in *Abstracts of the XXVII Radio Astronomy Conference, St. Petersburg* (1997), Vol. 1, p. 176.
33. B. H. Andrew, J. M. Macleod, G. A. Harvey, and W. J. Medd, Astron. J. **83**, 863 (1978).
34. H. D. Aller, M. F. Aller, G. Latimer, and P. E. Hodge, Astrophys. J., Suppl. Ser. **59**, 513 (1985).
35. H. Terasranta, M. Tornikoski, E. Valtaoja, *et al.*, Astron. Astrophys., Suppl. Ser. **94**, 121 (1992).

Translated by D. Gabuzda